Investigating the importance of strain-coupling in lead-free 2–2 relaxor/ferroelectric composites with digital image correlation

Alexander Martin[1,2,*] ⬤, Juliana G Maier[1] ⬤, Friedemann Streich[3] ⬤, Marc Kamlah[3] ⬤ and Kyle G Webber[1] ⬤

[1] Department of Materials Science and Engineering, Friedrich-Alexander-Universität Erlangen-Nürnberg, Erlangen 91058, Germany

[2] Department of Life Science and Applied Chemistry, Graduate School of Engineering, Nagoya Institute of Technology, Nagoya 466-8555, Japan

[3] Institute for Applied Materials (IAM-WBM), Karlsruhe Institute of Technology, Eggenstein-Leopoldshafen 76344, Germany

E-mail: martin.alexander@nitech.ac.jp

Abstract

Ceramic–ceramic composite structures are a viable solution to improve the electromechanical response of lead-free ferroelectrics (FEs) through tuning of the local electrical and mechanical fields. The origin of the enhanced properties, however, remains unclear, as many of the possible effects, such as polarization and strain coupling (PSC) as well as interface diffusion, are interrelated and difficult to separate or directly investigate. In this study, we use a custom-built digital image correlation system to directly investigate the influence of strain coupling on 2–2 composites consisting of $0.90Na_{1/2}Bi_{1/2}TiO_3–0.06BaTiO_3–0.04K_{0.5}Na_{0.5}NbO_3$ (NBT–6BT–4KNN) and $0.94Na_{1/2}Bi_{1/2}TiO_3–0.06BaTiO_3$ (NBT–6BT) by varying the mechanical interface contacts between end members. Specifically, two model cases were utilized to separate the relative contributions of the PSC mechanisms: (a) electrically connected and (b) mechanically and electrically connected. The local strain gradient was characterized through the thickness of the composite across different layers as well as the interface, where the macroscopic large signal longitudinal and transverse FE response was determined. Experimental results reveal an enhancement of the large signal piezoelectric coefficient d_{33}^* by approximately 10% from 390 to 440 pm V^{-1} due to strain coupling.

Keywords: ferroelectric relaxor, composites, digital image correlation, interface

(Some figures may appear in color only in the online journal)

1. Introduction

In order to replace lead-containing ferroelectric (FE) materials due to environmental and health concerns, a number of lead-free material systems have been identified, such as (K, Na) NbO$_3$ (KNN)-based [1], Na$_{1/2}$Bi$_{1/2}$TiO$_3$ (NBT)-based [2], and BaTiO$_3$ (BT)-based [3] materials. Among them, the (Na$_{1/2}$Bi$_{1/2}$)TiO$_3$–BaTiO$_3$ (NBT–BT) system, in particular in the vicinity of the morphotropic phase boundary (MPB) at a BT-content of approximately 6–7 mol% that separates the rhombohedral NBT and tetragonal BT phases

[4–6], has demonstrated exceptionally large unipolar strains that are of interest for actuation systems. Subsequently, Zhang *et al* demonstrated a giant electric-field-induced strain through the introduction of an additional end member that was able to modulate the thermal stability of the nonergodic–ergodic relaxor (RE) transition through destabilization of the electrically induced long-range FE order [5, 7, 8].

NBT–BT near the MPB is a non-ergodic RE at room temperature, arising due to the lack of chemical order, which is supported by both analytical [9–11] and experimental [7, 8, 10–16] investigations. This chemical heterogeneity can result in the formation of local polar nanoregions, which are embedded in a nonpolar matrix. Transmission electron microscopy (TEM) observations by Cheng *et al* [17, 18] have found a core–shell structure consisting of a nanosized tetragonal core embedded in a cubic shell in $(Na_{1/2}Bi_{1/2})TiO_3$–$0.026BaTiO_3$–$0.12(Bi_{0.5}K_{0.5})TiO_3$. Despite this local perovskite structure, *in situ* diffraction studies have demonstrated that NBT–7BT lacks a long-range FE order in the virgin state typical of perovskite FEs [19]. However, during the application of an electric field, a field-induced transformation to a meta-stable lower-symmetry phase is observed [19], corresponding to the formation of metastable FE domains [5, 6, 20, 21] and the development of a large polarization and strain response. This is understood to be a field-induced transition from the RE state to a metastable long-range FE order. With increasing temperature, however, the metastable FE order can be thermally destabilized. In the vicinity of the critical temperature T_{F-R}, which separates the ergodic and non-ergodic RE states [22, 23], the remanent polarization and strain is reduced through the loss of metastability and the spontaneous transition back to the macroscopic non-polar state during removal of the electric field [23, 24]. Through the reversibility of the electric-field induced phase transformation, large differences between maximum and remanent polarization and strain are achieved, resulting in a large electromechanical response. Importantly, the metastability of the long-range FE order can be chemically tuned using relatively small amounts of various end members. For example, Zhang *et al* [2] modified the NBT–BT system with KNN forming the solid solution $(Na_{1/2}Bi_{1/2})TiO_3$–$BaTiO_3$–$(K_{0.5}Na_{0.5})NbO_3$ (NBT–BT–KNN), effectively shifting the T_{F-R} to room temperature and resulting in large electric-field-induced strains of up to 0.45% [23].

Despite the potential of ergodic RE materials, the relatively large electric fields required to induce long-range FE order as well as the significant hysteresis limit their potential integration into applications. Thus, an important goal is to reduce the critical electric field required to induce long-range FE order, referred to as the poling field E_{pol}, while maintaining a large strain. One proposed method to reduce the poling field is through the development of ceramic–ceramic composites, which has been previously investigated by Dausch *et al* for lead-based FE–antiferroelectric (FE–AFE) composites [25, 26]. They observed a reduction of the required electric field for the phase transition from AFE to FE by the presence of FE phase in an AFE matrix, where the critical

electric field as a function of FE content was estimated by using a two-serially-connected capacitor model. In this case, the polarizations in the capacitors were assumed to be coupled, meaning that the macroscopic electrical response of the capacitors influence one another. As both end members showed different macroscopic polarization-electric field responses, there was assumed to be a local redistribution of the applied electric field that caused a shift in the apparent critical field in the AFE component [27, 28]. This work, however, did not take the effect of strain coupling into account, where the mechanical interaction of the components can influence the electromechanical response. Subsequently, Lee *et al* [27, 28] showed an enhancement in the large field strain behavior for lead-free RE/FE 0–3 type composites (phase assembly nomenclature by Newnham [29]), demonstrating that the composite structure not only provides a reduction of the driving electric field but also yields an enhanced strain by tailoring the contents of the RE and FE phases. Later, Groh *et al* showed similar results for $0.92(Na_{1/2}Bi_{1/2})TiO_3$–$0.06BaTiO_3$–$0.02K_{0.5}Na_{0.5}NbO_3$ and 0.93NBT–0.07BT (NBT–7BT) composites [30, 31].

Even though composites have demonstrated promising results, the underlying mechanisms are still not fully understood, such as the internal residual stresses and porosity arising from different sintering trajectories of the end members, interdiffusion between the constituents, and the influence of strain coupling. For this reason, studies on 2–2 composites have been conducted on different material systems to highlight certain aspects [32–35]. In particular, the work by Zhang *et al* [35] showed the importance of strain-coupling in multilayer composites of $0.91(Na_{1/2}Bi_{1/2})TiO_3$–$0.06BaTiO_3$–$0.03AgNbO_3$ and NBT–7BT by varying the orientation of the interfaces parallel and perpendicular to the applied electric field, where it was possible to remove the influence of the polarization coupling (PC). As a result, improvements of the electromechanical properties of the constituents were observed only for the strain-coupled samples, showing the influence of mechanical-coupling in addition to PC. Similar conclusions were reached by Ayrikyan *et al* [34] in two separate composite systems. For one NBT–7BT was combined with $(Na_{1/2}Bi_{1/2})TiO_3$–$25SrTiO_3$, where the enhancement could not only be attributed to PC, but also to strain coupling between the constituents. Further studies also showed that the interdiffusion between the constituent materials can change with the volume fraction of the seed material, as well as the stresses during sintering and the resulting residual stress. These changes at the interface can have an overall impact on the composite, as it changes the mechanical properties around the interface, together with increased pore fraction, increased grain size, and changes to the crystallographic structure [32, 33]. For instance, as pores have a relative permittivity of 1, charge accumulation during the application of an electric field can occur at the interface between the pore and the FE, resulting in a localized large electric field. As a result, the bilayer composition of NBT–7BT with 20 vol% $0.94Bi_{0.5}(Na_{0.75}K_{0.25})0.5TiO_3$–$0.06BiAlO_3$ showed

the highest increase in pore size and therefore also the highest strain response as shown by Ayrikyan *et al* [32].

To date, strain measurements on such composites were performed by using techniques that capture the average strain response of the entire composite and ignore the inherent inhomogeneous strain fields observed through the composite structure. This is especially true for observations near the interface that separates the constituent members, thereby limiting the understanding of the mechanisms responsible for the electromechanical coupling in ceramic–ceramic composites. Here, the digital image correlation (DIC) method can directly provide full-field displacements to sub-pixel accuracy and full-field strains during deformation through an applied external electrical field [36, 37]. The DIC method allows for the direct investigation of a region of interest on a test object surface, making this technique a highly effective tool suitable for monitoring the local deformations in ceramic–ceramic composites. In this work, NBT–6BT–4KNN and NBT–6BT were used as RE and FE materials, respectively. The 2–2 RE/FE bilayer composites with varying RE and FE volume fractions were prepared to directly investigate the polarization and strain coupling (PSC) effects by modifying the electrical and mechanical boundary conditions of the composites. The DIC method was used to study the local strain fields of each layer of the RE/FE multilayer composite as well as the interface region during electric field loading.

2. Experimental methodology

NBT–6BT–4KNN and NBT–6BT powders were produced via solid oxide synthesis route and chosen for RE and FE material for the bilayer structure, respectively. The used starting powders were Bi_2O_3 (99.975% purity, Alfa Aesar), TiO_2 (99.6% purity, Alfa Aesar), Na_2CO_3 (99.95% purity, Alfa Aesar), K_2CO_3 (99.95% purity, Alfa Aesar), Nb_2O_5 (99.95% purity, Alfa Aesar), and $BaCO_3$ (99.95% purity, Alfa Aesar). The powders were mixed according to their stoichiometric formula and milled together with ZrO_2 balls in ethanol for 24 h, followed by calcination at 800 °C for 2 h. The final powders were uniaxially pressed and subsequently cold-isostatically pressed at −180 MPa. Afterwards, the green bodies were sintered at 1150 °C for 3 h using powder of same composition for sacrificial purposes, where the heating and cooling rate was 3 K min^{-1}. Samples were cut and ground to rectangular samples with a surface area of 4 mm × 4 mm using a surface grinder. In order to produce bilayers with varying volume fractions of the RE and FE end members, the height of the individual components was adjusted accordingly, where the total height of the bilayer was fixed to 4 mm. During this investigation, bilayers with a volume ratio 0, 50, and 100 vol% seed were measured. The surfaces of the samples were sputtered with gold to create electrodes and the samples were annealed at 500 °C for 1 h in order to reduce internal stresses and stress-induced FE phases that occurred during sample preparation.

During electrical testing, two different cases were used: case (a), where the samples were stacked with a series electrical connection via the gold electrodes but without a mechanical connection, assuming to lead to only PC and case (b), where both layers were electrically connected in series and also mechanically joined by gluing via silver paste, assuming to lead to PSC (figure 1(b)). It is important to note that the effects of friction in case (a) were assumed to be negligible, meaning that the samples were assumed to independently deform without mechanical constraints from the measurement system or the adjoining sample. In order to measure the electromechanical responses of the bilayer samples, the measurement setup as shown schematically in figure 1 was used, which was comprised of a Sawyer–Tower circuit with a reference capacitor C_{ref} of 4.9 nF to measure the electric field dependent polarization as well as a linear variable differential transformer (LVDT) to record the total strain of the bilayers. A glass window was attached to the sample holder, which was made of Teflon, and allowed to be used as oil bath to avoid overarching during electrical testing. The sample holder, positioning system, and LVDT holder were designed, and built in-house. Electric fields with a triangular waveform using a maximum value of ±4 kV mm^{-1} and a loading rate of 0.08 kV mm^{-1} s^{-1} (0.1 Hz) were applied parallel to the three-direction with a high-voltage power supply (Trek Amplifier, Model 20/20C); a custom-built LabVIEW program was used as a waveform generator and a data recording and analysis program for the polarization and LVDT strain measurements. Importantly, measurements were started from the virgin, unpoled state, providing information on the remanent strain development during electric field loading.

In order to directly observe the electromechanical response of the different layers, a digital camera (MC089MG-SY-UB, Ximea GmbH) with a resolution of 4112 × 2176 pixels that imaged one side of the sample for the DIC system was used. Combined with a lens with 2× magnification (MVO-TML Telecentric Measuring Lens, Edmund Optics Inc.), a resolution of 1.75 μm pixel^{-1} could be achieved. Artificial speckles were sprayed onto the observation surfaces by means of an air brush (AT-Airbrush Pistole Kit, AT-AK-02, Agora-Tec), thus allowing the creation of patterns suitable for DIC tracking. The camera captured two images per second to record the deformation during electric field loading. The images were analyzed using a commercially available DIC-program, Veddac (version 6.0). Here, a distance of 60 pixel or 105 μm between the measurement points as well as a reference field of 120 × 120 pixel were used. Additionally, the hair wavelet function was chosen to increase accuracy and minimize the standard deviation between points. Using this technique, the strain field was characterized as a function of position through the thickness of the sample by averaging the strain values along a line parallel to the interface. To measure the noise, images of the sample were taken for 100 s without the application of an electric field while using the same DIC parameters. A background noise level of 0.04 pixels or approximately 0.002% was observed.
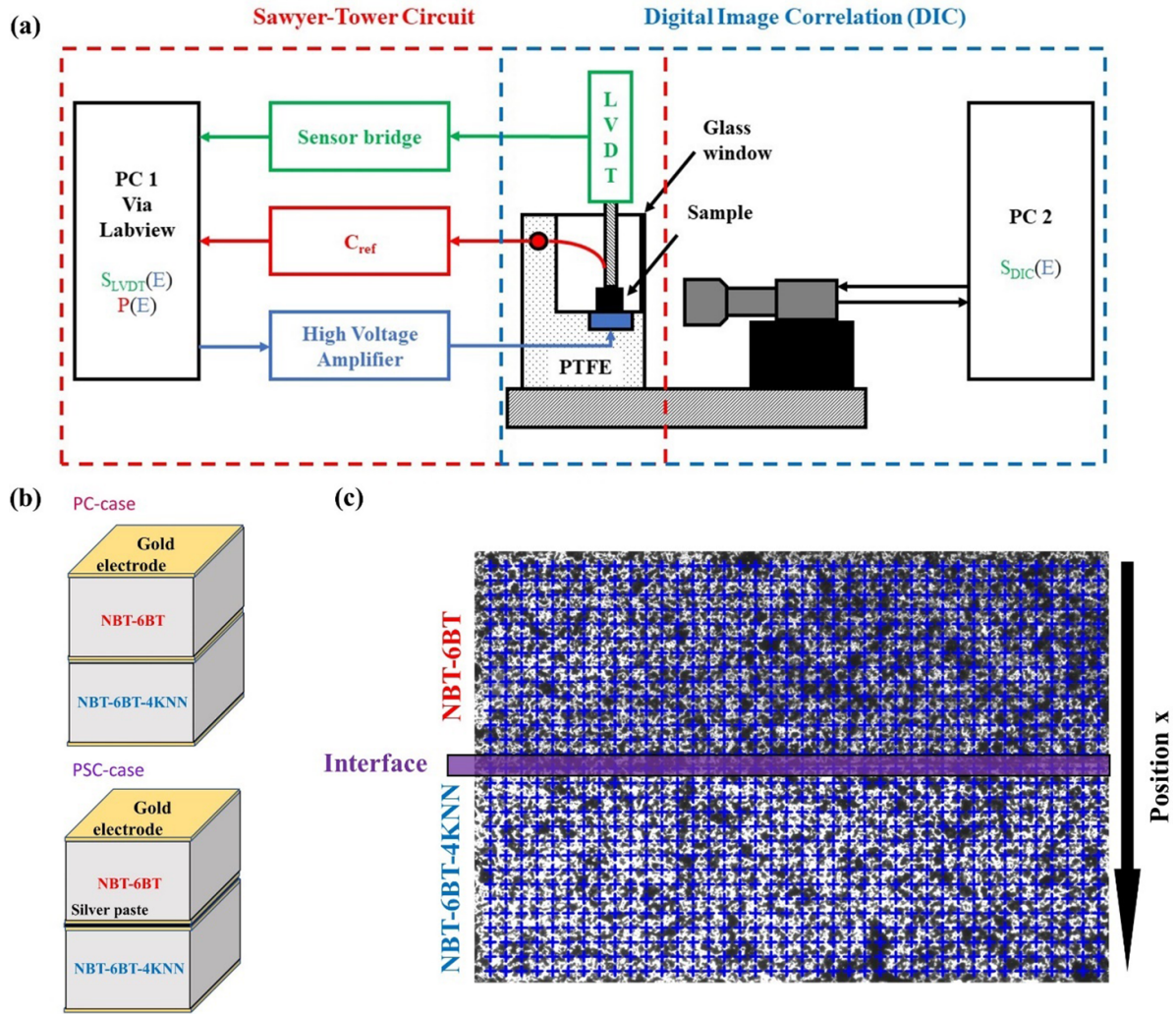
Figure 1. Schematics of the experimental setup, which combines overall polarization and strain measurements with spatial resolution of the strain via DIC (a). Schematic representation of the PC and PSC case (b). The amount of measurement points across the bilayer sample, as used during the DIC measurement (c).

3. Results and discussion

The DIC measurement system was used to characterize the macroscopic longitudinal and transverse strain response of the end members NBT–6BT and NBT–6BT–4KNN as well as their ceramic–ceramic composites with both PC and PSC connectivity (figure 2). It is important to note that slight differences can occur due to changes in lighting during measurement, from e.g. minor vibrations or silicone oil movement, that can affect the images used for DIC analysis. In particular, silicone oil, which was used as an electrical insulating liquid during the high voltage experiments, was found to move during the application of an electric field, resulting in minor variations of the light exposure from image to image that increased error. This error was minimized by locating the sample as close as possible to the glass window to reduce the volume of silicone oil between the sample surface and the camera and limiting the electrical loading frequency. Importantly, despite the increased local error in the determination of strain fields, the average value of a larger region was found to provide accurate

strain results. To ensure accuracy of the strain results from the DIC analysis, they were directly compared to longitudinal strain measurements from an LVDT, where an excellent agreement is observed (figure 2).

NBT–6BT shows a typical non-ergodic RE strain-electric field hysteresis response with a large remanent ($S_{rem} = 0.25\%$) and maximum strain ($S_{max} = 0.36\%$). To calculate the large signal piezoelectric coefficient d_{33}^* and d_{31}^*, the maximum and remanent strain were subtracted and divided by the maximum electric field ($S_{max} - S_{rem}/E_{max}$), which was 4 kV mm^{-1} for each case. In addition, for the d_{33}^* the longitudinal strain (S_{33}), and for d_{31}^* the transverse strain (S_{11}) was used. This resulted in a d_{33}^* and d_{31}^* of approximately 250 and -112 pm V^{-1} for NBT–6BT, respectively. In addition, during initial electric field loading from the virgin state, a significant jump in longitudinal and transverse strain is observed at the poling field ($E_{pol} = 2.3$ kV mm^{-1}), defined as the inflection point during the first increase of the electric field and describes the critical electric field to induce a transition from the RE state to long-range FE order. In contrast, NBT–6BT–4KNN
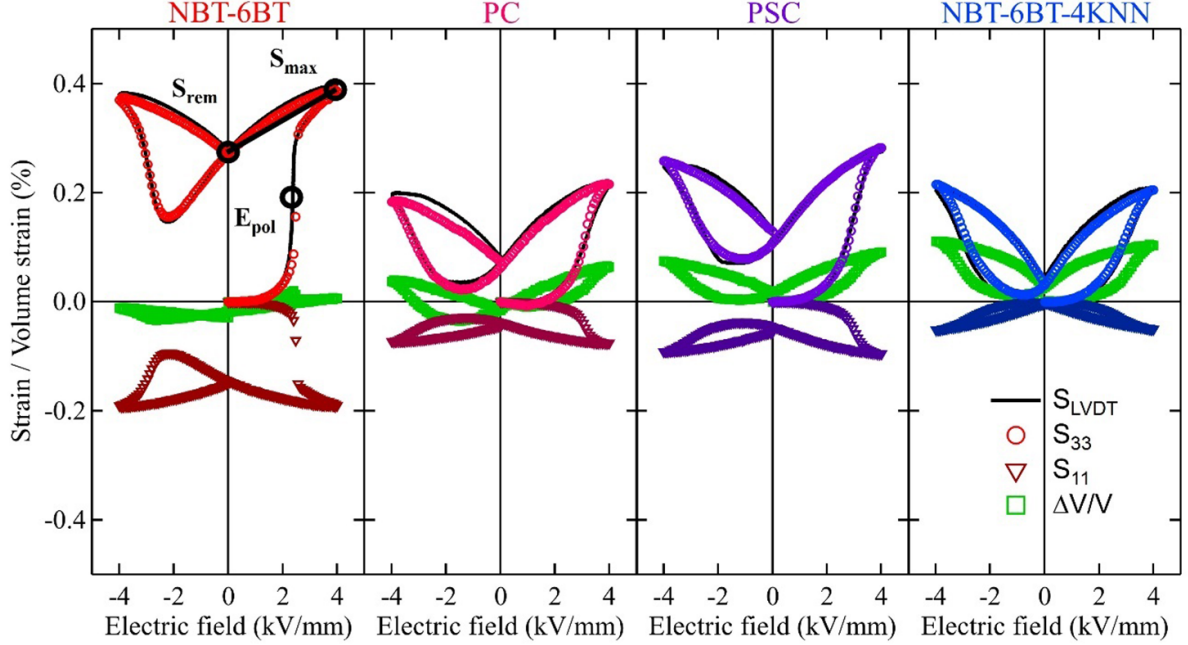
Figure 2. The longitudinal strain (S_{33}) and transverse strain (S_{11}) as well as the resulting volumetric strain ($\Delta V/V$) as a function of electric field for NBT–6BT, PC, PSC, and NBT–6BT–4KNN. The longitudinal strain data determined with the DIC system was compared to an LVDT, shown as a black line, indicating close correlation between both measurement methods.

did not display a significant remanent strain development (0.05%). However, due to this and the relatively high maximum strain ($S_{max} = 0.21\%$), the large signal piezoelectric coefficient was found to be nearly 56% larger than for NBT–6BT ($d_{33}^* = 390\,\mathrm{pm\,V^{-1}}$, $d_{31}^* = -120\,\mathrm{pm\,V^{-1}}$). The poling field for NBT–6BT–4KNN was found to be 2.7 kV mm^{-1}.

Importantly, the DIC method also allows the simultaneous characterization of the strain perpendicular to the applied electric field (S_{11}), which is also shown in figure 2. In all cases, the transverse strain mirrors the form of the longitudinal strain (S_{33}), where the magnitude is approximately half the longitudinal value for NBT–6BT and a fourth for NBT–6BT–4KNN. By combining the strain components, S_{33} and S_{11}, it is possible to directly characterize the volume strain during electric field loading [38]. Assuming a transversely isotropic electromechanical response, the volume strain can be measured with the following equation:

$$\frac{\Delta V}{V} = \frac{(c + \Delta c)(a + \Delta a)^2 - ca^2}{ca^2}. \tag{1}$$

Here, c describes the height of the sample and a the width and depth, resulting in the following equation when solving for the longitudinal and transverse strain:

$$\Delta V/V = (1 + S_{33})(1 + S_{11})^2 - 1. \tag{2}$$

As the strains are small, the products of the strains with each other (for instance $S_{33}S_{11}$) will be negligibly smaller than the strains itself, and the volumetric strain in that case is given by:

$$\Delta V/V \cong S_{33} + 2S_{11}. \tag{3}$$

During the application of an electric field, changes in, e.g. the crystal symmetry, domain state, or defect network result in the formation of local strains. Importantly, some of these effects are volume conserving, such as domain wall motion [39], whereas others, such as field induced structural phase transitions, can be driven by changes in volume [40]. It is important to note, however, that although field induced structural phase transitions can also be induced by deviatoric stress components, e.g. in potassium bicarbonate (KHCO$_3$) [41], such structural transitions are understood to be coupled to a change in volume between crystal phases in perovskite FE oxides. RE FEs undergo either a reversible or irreversible field induced phase transformation to long-range FE order. Previous studies have shown that remanent volume strains can occur in NBT–BT compositions that are related to the coalescence of nanopolar regions [38]. In this study, NBT–6BT does not show significant volume strain, suggesting that the transformation involves no crystallographic symmetry change. These results are consistent with the work of Jo *et al* [38], who measured the volume strain of NBT–BT with changing BT content. In contrast, NBT–6BT–4KNN displays a maximum volume expansion of approximately 0.1%, indicating the presence of a field-induced phase transformation.

Interestingly, the composite samples in figure 2 show a strain response between the end members, in terms of the maximum and remanent strain as well as the critical poling field, which was found to depend on the mechanical coupling. For the electrically connected sample (PC), where both components were able to freely move without mechanical constraint, a remanent and maximum strain of 0.07% and 0.20% were observed, respectively. Importantly, assuming a simple rule of mixtures, a remanent strain of 0.15%
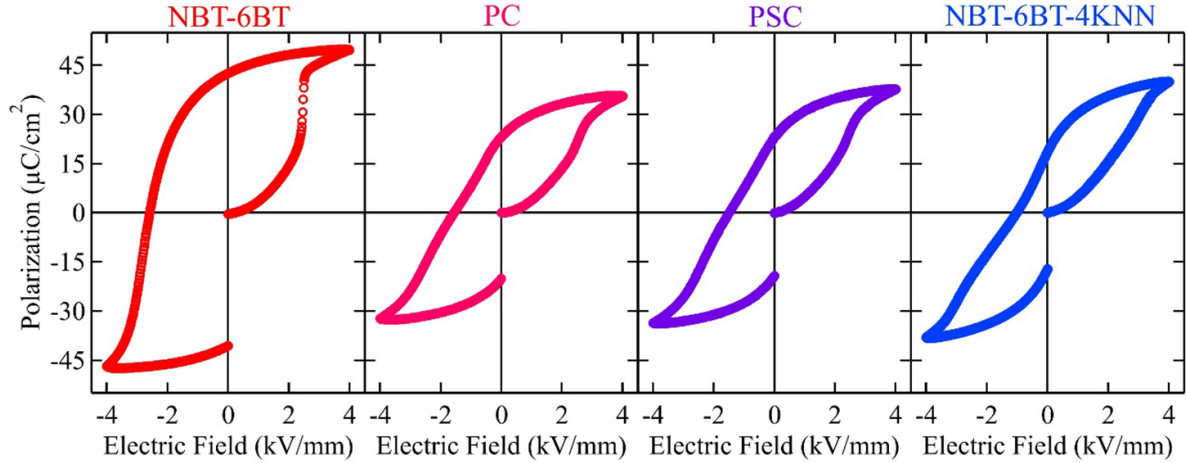
Figure 3. Results of polarization as a function of electrical field for NBT–6BT and NBT–6BT–4KNN, as well as the PC and PSC case.

would be expected, nearly twice that observed experimentally. Similarly, the poling field ($E_{pol} = 3.3$ kV mm^{-1}) was larger than that found in both end members, which suggests that the effective local electric field distribution required an increase in the externally applied electric field to induce the formation of a long-range order. These differences in applied and effective electric field seem to lead to an overall decrease of electromechanical properties, resulting in a d_{33}^* of 310 pm V^{-1} and a d_{31}^* of -100 pm V^{-1}.

When the end members are mechanically connected through a conductive interface (PSC), there is the formation of a strain coupling during electrical activation through the large signal d_{31}^* piezoelectric coefficient that can influence the electromechanical response of the composite. In this case, an increased maximum ($S_{max} = 0.28\%$), and remanent strain ($S_{rem} = 0.11\%$) as well as a decreased poling field ($E_{pol} = 2.6$ kV mm^{-1}) were observed compared to the electrically connected sample. This resulted in an increased d_{33}^* of 440 pm V^{-1}, as well, as an increased d_{31}^* of -128 pm V^{-1}. Both values show an enhancement of approximately 10% compared to NBT–6BT–4KNN, which had the highest values in between the end members. These results are consistent with the literature for 0–3 composites. As shown by Groh *et al*, NBT–BT/NBT–BT–KNN composites showed improved electromechanical behavior ($d_{33}^* = 500$ pm V^{-1}) at 50 vol.% NBT–6BT. It is important to note, however, that in addition to differences in end member connectivity, the samples in Groh *et al* were co-sintered, thus interdiffusion as well as internal stresses due to differences in the sintering behavior and coefficients of thermal expansion can also play an important role. Nevertheless, these results suggested a strong influence of strain coupling on the overall properties of the composite.

In addition to mechanical interactions, both end members are electrically connected through the PC effect, which, due to variations in the dielectric permittivity, electrical resistance, and large field polarization response, can affect the local distribution of the externally applied electric field. Figure 3 shows representative polarization-electric field hysteresis curves for the end members as well as the PC and PSC

bilayer composites. The matrix material NBT–6BT–4KNN displays a pinching behavior, typical for ergodic RE FEs [30, 42, 43], corresponding to low remanent polarization ($P_{rem} = 15$ μC cm^{-2}) and strain. In contrast, the seed material NBT–6BT, a non-ergodic RE, shows no apparent pinching effect and the formation of a large remanent polarization ($P_{rem} = 43$ μC cm^{-2}), characteristic for this system [44]. As such, the remanent polarization of the composite ($P_{rem} = 20$ μC cm^{-2}) increased with the addition of a non-ergodic RE component, similar to previous studies [28, 30]. This behavior is to be expected, as NBT–6BT has higher remanent and maximum polarization. Interestingly, both the PC and PSC cases display a similar polarization behavior, in contrast to the strain-response, which shows a significantly higher remanent strain for the PSC sample. This is suggested to be due to the strain coupling between end members, where the increased mechanical connectivity affected the macroscopic constitutive response.

In addition, the coercive fields can be determined from the polarization curves. These were 2.57, 1.56 and 1.49 kV mm^{-1} for NBT–6BT, the PC-case, and the PSC-case, respectively. It should be noted that these values differ from their poling fields ($E_{pol,NBT-6BT} = 2.3$ kV mm^{-1}; $E_{pol,PC} = 3.3$ kV mm^{-1}; and $E_{pol,PSC} = 2.6$ kV mm^{-1}). This difference is most likely caused by the differences in the kinetics for both processes. During the poling phase the material experiences a RE-to-FE order transition, whereas in the switching phase FE domain wall motion occurs. The different kinetics of both processes have been shown for instance on NBT–7BT [45], where different behavior depending on the applied rate of the electric field was shown.

When combining two capacitors in series, the charge and by extension the polarization for both capacitors must be equal, assuming infinite resistivity. In a system where the dielectric permittivity varies between each component, the local voltage on each capacitor is different and as a result, there is an inhomogeneous electric field distribution. To ensure equal polarization, an enhanced local electric field would be required in the NBT–6BT–4KNN layer, as NBT–6BT displays a larger
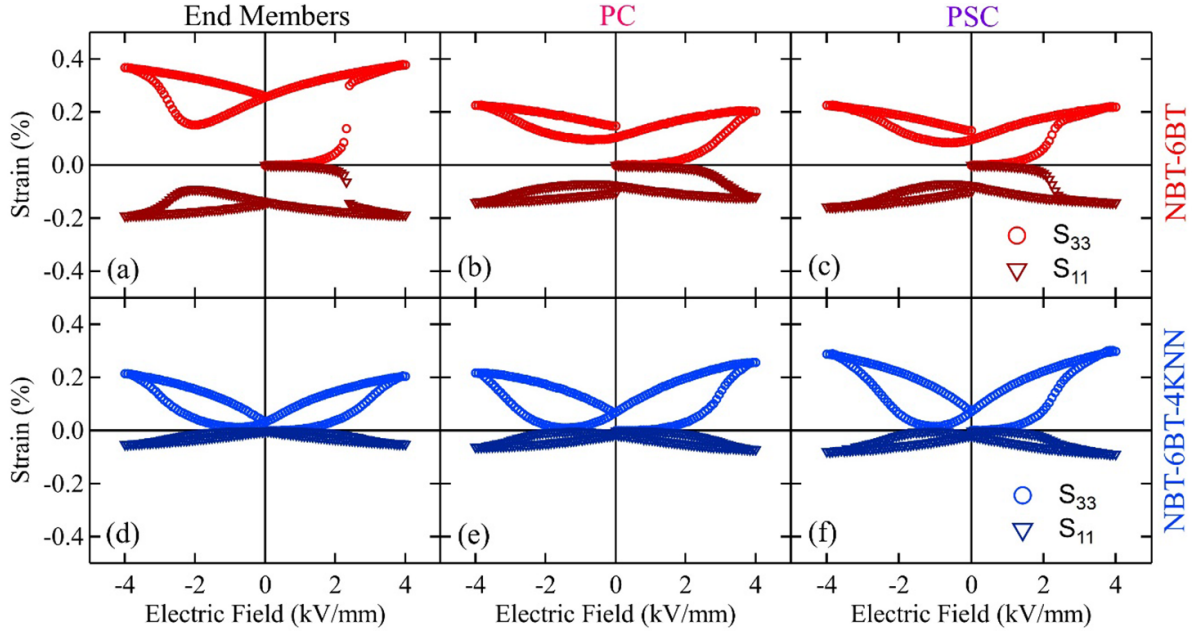
Figure 4. Strain-electric field hysteresis curves in longitudinal S_{33} and transverse S_{11} directions for end members NBT–6BT (a) and NBT–6BT–4KNN (d) as well as the NBT–6BT region in the PC and PSC configurations, (b) and (c), respectively, and the NBT–6BT–4KNN region in the PC and PSC configurations, (e) and (f), respectively. When testing individual regions, care was taken to remain at least 60 μm from the interface to ensure only the end member component of interest was investigated.

polarization, which is expected to promote the electric field induced long-range FE order in the ergodic RE component at lower external electric fields. This has been used in different investigations to increase the effective electric field in RE-based composites [27, 28, 30, 31]. Using these results and combining them with the uncoupled results of the NBT–6BT end member (figure 2), one could assume that NBT–6BT was not fully polarized during the measurement. This is suggested by the lower maximum and remanent polarization, as well as the higher poling field in the composite structure. In the PC case, it seemed the effective electric field on NBT–6BT was insufficient to polarize the sample and caused a significant decrease in the polarization. As such, there was no significant increase in the electric field in NBT–6BT–4KNN and the electromechanical properties. This appeared to have been the case in PSC as well, however one would need to observe each layer individually to fully verify this. As such, the DIC method was used to directly investigate the strain response for each component, thus allowing for more information about the influence of strain coupling on the local properties.

The local strain-electric field behavior for NBT–6BT and NBT–6BT–4KNN are presented in figure 4 for both the PC and PSC cases. Overall, the strain response for both end members change significantly when combining them in the ceramic–ceramic composite structures. In the case of NBT–6BT there is a decrease in the longitudinal remanent strain in both the PC and PSC configurations from 0.25% to approximately 0.11% and 0.10%, respectively. Alongside the decrease in the maximum strain of the PC (S_{33}) composites, a reduction of the electromechanical properties of NBT–6BT ($d_{33}^* = 170$ pm V^{-1}, $d_{31}^* = -87$ pm V^{-1}) was observed. Interestingly, despite the decrease in the maximum strain of the

PSC composites (S_{33}), almost no reduction in the PSC-case ($d_{33}^* = 235$ pm V^{-1}, $d_{31}^* = -117$ pm V^{-1}) occurred. It is important to note, that due to the redistribution of the applied electric field on the composite components, there was an apparent increase in the poling field of the PC sample to $E_{pol} = 3.3$ kV mm^{-1}. This is approximately 43% higher than that observed for NBT–6BT ($E_{pol} = 2.3$ kV mm^{-1}), resulting in a lack of saturation of the longitudinal and transverse strain (figure 4(b)). This is understood to be the origin of the reduced electromechanical response in the NBT–6BT end member of the PC sample. Interestingly, mechanical coupling in the PSC sample was found to decrease the poling field ($E_{pol} = 2.6$ kV mm^{-1}), in comparison to PC alone, to values comparable to that observed for the end member. Despite this, however, the remanent strain remained considerably lower compared to the uncoupled case, which is likely due to the mechanical constraints imposed by the NBT–6BT–4KNN layer.

Similarly, the local strain-electric field response of the NBT–6BT–4KNN layer was observed for both PC and PSC samples. NBT–6BT–4KNN is understood to be an ergodic RE at room temperature with a correspondingly low remanent strain, which is evident in the longitudinal and transverse strain behavior of the uncoupled sample (figure 4(d)). However, in both the PC and the PSC configuration there was an increase in the remanent and maximum strain, hysteresis, and negative strain, defined as the strain difference between the lowest strain and the remanent strain as well as a corresponding change in the poling field. Changes in the remanent and negative strain are likely due to the formation of internal bias fields that can be developed during PC [46]. Although residual mechanical fields could also affect the remanent state, in
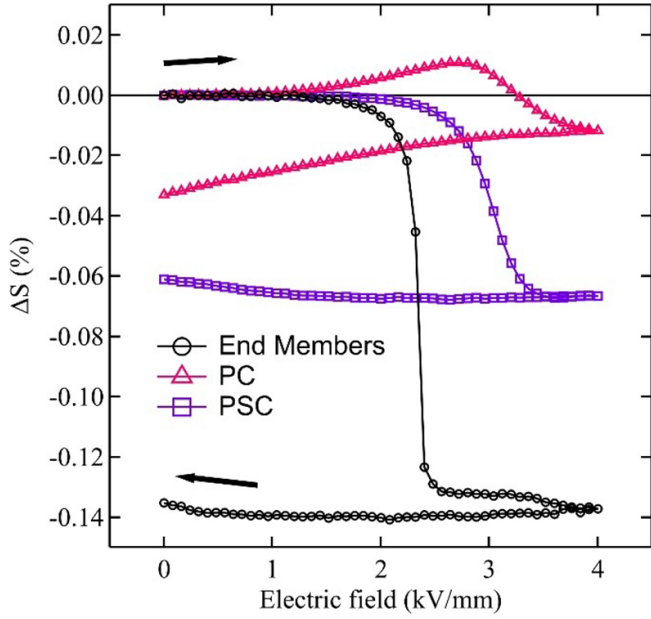
Figure 5. Strain difference between NBT–6BT and NBT–6BT–4KNN as a function of electric field.

particular considering the large transverse remanent strain in the NBT–6BT end members, it is not expected to play a significant role, as similar remanent strains are observed in both PC and PSC samples despite the lack of mechanical coupling in the PC state. Similar to observations in NBT–6BT, the PC sample displayed an increase in the poling field over the end member from 2.7 to 3.1 kV mm^{-1}, whereas the PSC sample decreased to 2.6 kV mm^{-1}. This resulted in a decrease in the electromechanical properties for the PC case ($d_{33}^* = 377$ pm V^{-1}, $d_{31}^* = -104$ pm V^{-1}) and an increase for the PSC case ($d_{33}^* = 490$ pm V^{-1}, $d_{31}^* = -124$ pm V^{-1}). Note that NBT–6BT–4KNN itself shows a higher d_{33}^* than the overall composite in the PSC case ($d_{33}^* = 440$ pm V^{-1}), as the overall strain also is dependent on the electromechanical response of NBT–6BT. These results clearly demonstrate the importance of strain coupling in enhancing the strain response of ceramic–ceramic composite structures.

Interestingly, the composite structure was not found to significantly affect the poling field in either the NBT–6BT or the NBT–6BT–4KNN end members in the PSC sample. In order to investigate this, the strain difference between NBT–6BT and NBT–6BT–4KNN are measured from the virgin state as a function of the electric field for the PSC and PC cases, where the S_{11} strain difference between end member materials was determined ($\Delta S_{11} = S_{11,\text{NBT}-6\text{BT}} - S_{11,\text{NBT}-6\text{BT}-4\text{KNN}}$), providing information on the formation of internal biaxial stress during the application of an electric field. This strain difference is shown in figure 5 as a function of electric field. When comparing the values of the end members in the uncoupled case, up to 2 kV mm^{-1}, no significant change occurs, as both materials do not expand in that region. However, at 2 kV mm^{-1} NBT–6BT contracts sharply, resulting in a strain difference of approximately

−0.14%. Interestingly, in the PC sample, the strain difference initially increases positively before decreasing sharply, suggesting that NBT–6BT–4KNN initially contracts before NBT–6BT. The reason hereby might be the change in the effective electric field, suggesting a larger effective electric field in NBT–6BT–4KNN and a lower effective electric field in NBT–6BT, when comparing to the non-composite case. Subsequently to this positive strain difference, however, the development of a large remanent strain in NBT–6BT and the corresponding transverse strain result in large strain gradient between end members above approximately 3 kV mm^{-1}. In the strain coupled case, no significant strain difference was observed below 2 kV mm^{-1}, followed by a significant increase in the strain difference above 2 kV mm^{-1}. Considering the same effective electric fields as in the PC-case, this curve shows the strain coupling in effect. NBT–6BT–4KNN experiences a larger effective electric field compared to NBT–6BT, thus seems to contract before NBT–6BT, as suggested by the PC-curve. However, due to strain coupling, NBT–6BT contracts at first similar to NBT–6BT–4KNN, which is why the strain difference remains constant at 0 until approximately 2.3 kV mm^{-1}. Furthermore, the results suggest a lower poling field for NBT–6BT in the PSC case compared to the PC case, as the significant decrease in the strain difference occurs before the PC case. One possibility is due to biaxial compression on NBT–6BT, caused by the early contraction of NBT–6BT–4KNN as suggested by the PC case. The influence of biaxial/radial stress on the poling of FE materials has been previously reported, where a decrease in the poling field was observed [47, 48]. Nevertheless, it should be noted that the poling field in the PSC case is still higher than in the non-composite case, further proofing the lower effective electric field in NBT–6BT.

During the unloading phase, the PC case continues to increase in the strain difference from −0.01% to −0.03%. On the other hand, in the PSC case NBT–6BT, as well as NBT–6BT–4KNN, seem to expand at the same rate, thus an almost constant strain difference of −0.06% between them remains. This is due to the way the end members are connected in each case. In the PC case, both end members can freely move without any constraints whereas in the PSC case they are mechanically connected. As such, in the PSC case, as long as there in no significant deviation between the electric-field induced strain in NBT–6BT and NBT–6BT–4KNN, strain coupling occurs and the strain difference remains constant. This was the case in the beginning of the application of the electric field as well as during unloading of the sample.

In the initial, electrically unpoled state the internal residual stresses are zero, as each end member was combined at room temperature. However, during and following the application of an external electric field, the internal stress in the PSC composite will change depending on the transverse electromechanical response, including both the small signal transverse piezoelectric coefficient d_{31} as well as the macroscopic lateral strain d_{31}^*. In particular, the internal residual stresses remain once the electric field has been removed, as both end members display differences in transverse remanent strain. In order to demonstrate this effect, figure 6 shows the strain as a function of the
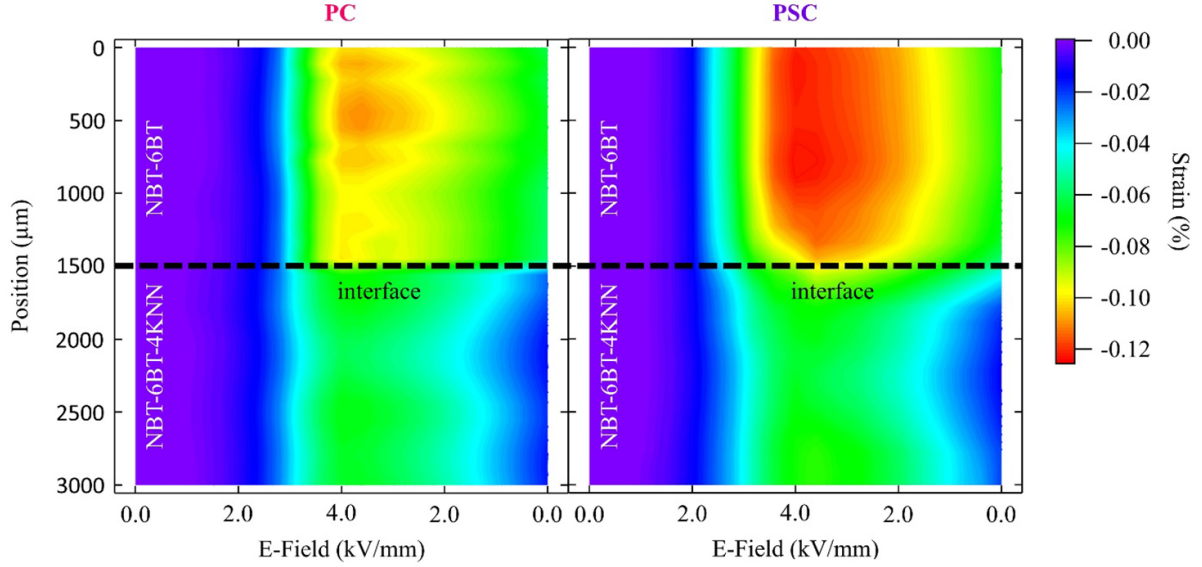
Figure 6. Strain as a function of position for the PC and PSC case for different electric field steps. The black line at 1500 μm signalizes the interface between NBT–6BT and NBT–6BT–4KNN.

position through the cross-section of the composite structure for both the PC and the PSC cases. In the initially unpoled state, there is no strain gradient through the thickness of either configuration. However, with the application of an electric field, a significant increase in the strain gradient is observed. A sharp jump in strain is observed in the PC configuration when increasing the electric field over approximately 3.5 kV mm^{-1}, as no mechanical connection is present between the two end members. Importantly, however, the strain within each layer is uniform, displaying no significant gradient or variation within the resolution of the present measurements. This is the case for increasing the electric field as well as during decreasing. In contrast, the mechanical interface in the PSC case resulted in a more gradual, continuous strain transition through the thickness of the composite structure. In particular, this is visible after unloading, where the NBT–6BT–4KNN sample shows a remanent strain close to the interface.

These data show that the strain gradient at the interface has a penetration depth into the end members of approximately 500 μm, after which a constant average strain is observed. Here, care was taken to select an appropriate reference field size for the DIC analysis. The reference field describes the size of the section at each measurement point, which will be searched via comparison to the subsequent images. The shift of this reference section thereby describes the displacement at that area. As such, if chosen too large, for example, the reference field would have gathered displacement information of the other material, resulting in an average value between the two, whereas too small would result in a larger error, as the reference field would contain less information for the comparison. Through experimentation, it is found that a reference field of 120 × 120 pixel or 204 × 204 μm resulted in reliable data. An additional possible source for error is the plastic deformation of the silver bond during the experiment. Using the DIC-results, a shear strain at the interface of about

0.18% was calculated, which is in the elastic region for similar silver paste-based adhesives [49–51]. We therefore assume that the plastic deformation of the silver is minor. The results seem therefore to be a real effect caused by the strain coupling between the materials. *In situ* electric field dependent x-ray diffraction as a function of position would help to understand the relaxation process that leads to changes in the strain gradient with position.

At a sufficient distance to the interface, the strain is constant and describes bulk strain behavior of the constituent material. For the PSC sample, both materials show a deviation from this macroscopic strain behavior at the interface. As such, calculating the difference ($\Delta S = S_{11,0} - S_{11,X}$) between the average bulk strain $S_{11,0}$ and the strain at each position $S_{11,X}$, one can assume the mechanical stress via the elastic properties, such as the Young's modulus, at the interface. This difference in strain is shown in figure 7 as a function of position across the interface. Closer to the interface the difference becomes negative for NBT–6BT–4KNN and positive for NBT–6BT. A positive ΔS suggests that the material contracted less at the interface than the normalized case, resulting in tensile stress. A negative ΔS on the other hand suggests a stronger contraction at the interface and by extension a compressive stress. In order to estimate the stresses, an isotropic, linear elastic response was assumed. The elastic modulus for NBT–6BT was found in previous investigations to be 105 GPa [52, 53]. For NBT–6BT–4KNN, however, the elastic modulus was assumed to be approximately 113 GPa [53], based on values reported for NBT–6BT–2KNN. This variation in elastic properties would help to explain the larger strain difference in NBT–6BT, as a smaller elastic modulus would require a larger strain for force equilibrium. Using these elastic properties, a maximum residual stress of approximately 40 MPa was estimated at the interface. It should be noted that the residual stress could be quite different as a constant strain does not
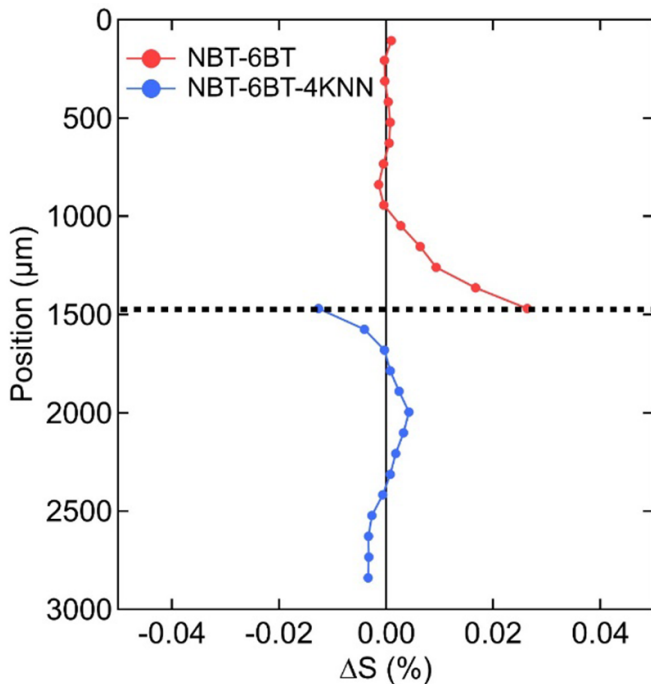
Figure 7. Strain difference between the constant strain and strain at interface as a function of position at an electric field E of 4 kV mm^{-1} in the PSC case. The black dotted line at 1500 μm represents the interface of the bilayer composite between NBT–6BT and NBT–6BT–4KNN.

necessarily mean a stress-free region. Nevertheless, the results suggest that there is residual stress in the material and *in situ* x-ray diffraction through the layers could directly confirm the stress profile as well as the magnitude. Combined with the previous results, this residual stress is responsible for the enhanced electromechanical properties [47, 48]. For instance, Kounga *et al* have shown that through radial compressive stress assisted poling, a higher piezoelectric charge coefficient in PZT could be achieved. It should be mentioned that this improvement, however, was decreased after the mechanical load was removed, suggesting an improvement only by constant mechanical stress, which is the case in our setup. As such, NBT–6BT–4KNN showed higher piezoelectric properties in the PSC case ($d_{33}^* = 490$ pm V^{-1}) compared to the uncoupled sample ($d_{33}^* = 390$ pm V^{-1}). On the other hand, NBT–6BT, which is in tensile stress, showed an overall lower piezoelectric strain decreasing from initial 250 to 235 pm V^{-1}.

4. Conclusion

The influence of electrical and mechanical interactions in bilayer composite structures of NBT–6BT and NBT–6BT–4KNN has been directly investigated using the DIC method. Experimental results indicate that PC alone does not result in an overall improvement of the electromechanical properties with the selected end members. However, with the addition of strain coupling between the layers, an overall enhancement of approximately 10% was achieved. The DIC method, through

in situ characterization of the local strain response of each end member, revealed that NBT–6BT was not fully polarized with only PC. As a result, high polarization values could not be achieved and the enhancement via PC was diminished. Through the introduction of mechanical coupling, however, the internal residual stresses developed due to the transverse electromechanical response induced a stress that enhanced the polarization of NBT–6BT. Subsequently, the sharp contraction of NBT–6BT results in a compressive stress in the NBT–6BT–4KNN layer that improves the longitudinal strain behavior.

ORCID iDs

Alexander Martin ⓘ https://orcid.org/0000-0002-6218-8390
Juliana G Maier ⓘ https://orcid.org/0000-0002-9044-1998
Friedemann Streich ⓘ https://orcid.org/0000-0002-4252-2013
Marc Kamlah ⓘ https://orcid.org/0000-0002-5710-1529
Kyle G Webber ⓘ https://orcid.org/0000-0002-1283-7874

References

[1] Li J-F, Wang K, Zhu F-Y, Cheng L-Q and Yao F-Z 2013 *J. Am. Ceram. Soc.* **96** 3677
[2] Zhang S-T, Kounga A B, Aulbach E, Ehrenberg H and Rödel J 2007 *Appl. Phys. Lett.* **91** 112906
[3] Liu W and Ren X 2009 *Phys. Rev. Lett.* **103** 257602
[4] Takenaka T, Maruyama K and Sakata K 1991 *Jpn. J. Appl. Phys.* **30** 2236
[5] Picht G, Töpfer J and Hennig E 2010 *J. Eur. Ceram. Soc.* **30** 3445
[6] Ma C, Guo H, Beckman S P and Tan X 2012 *Phys. Rev. Lett.* **109** 107602
[7] Viehland D, Jang S J, Cross L E and Wuttig M 1992 *Phys. Rev. B* **46** 8003
[8] Naberezhnov A, Vakhrushev S, Dorner B, Strauch D and Moudden H 1999 *Eur. Phys. J. B* **11** 13
[9] Pirc R and Blinc R 1999 *Phys. Rev. B* **60** 13470
[10] Cross L E 1987 *Ferroelectrics* **76** 241
[11] Viehland D and Cross L E 1991 *Phys. Rev. B* **43** 8316
[12] Vakhrushev S B and Shapiro S M 2002 *Phys. Rev. B* **66** 214101
[13] Jeong I-K, Darling T W, Lee J K, Proffen T, Heffner R H, Park J S, Hong K S, Dmowski W and Egami T 2005 *Phys. Rev. Lett.* **94** 147602
[14] Novak N, Pirc R, Wencka M and Kutnjak Z 2012 *Phys. Rev. Lett.* **109** 1
[15] Randall C A, Bhalla A S, Shrout T R and Cross L E 1990 *J. Mater. Res.* **5** 829

[16] Gehring P M, Hiraka H, Stock C, Lee S-H, Chen W, Ye Z-G, Vakhrushev S B and Chowdhuri Z 2009 *Phys. Rev.* B **79** 24
[17] Cheng S-Y, Shieh J, Ho N-J and Lu H-Y 2011 *Phil. Mag.* **91** 4013
[18] Cheng S Y, Shieh J, Lu H Y, Shen C Y, Tang Y C and Ho N J 2013 *J. Eur. Ceram. Soc.* **33** 2141
[19] Daniels J E, Jo W, Rödel J and Jones J L 2009 *Appl. Phys. Lett.* **95** 032904
[20] Schmitt L A, Kling J, Hinterstein M, Hoelzel M, Jo W, Kleebe H-J and Fuess H 2011 *J. Mater. Sci.* **46** 4368
[21] Garg R, Rao B N, Senyshyn A, Krishna P S R and Ranjan R 2013 *Phys. Rev.* B **88** 014103
[22] Foronda H, Deluca M, Aksel E, Forrester J S and Jones J L 2014 *Mater. Lett.* **115** 132
[23] Jo W, Dittmer R, Acosta M, Zang J, Groh C, Sapper E, Wang K and Rödel J 2012 *J. Electroceram.* **29** 71
[24] Jo W, Granzow T, Aulbach E, Rödel J and Damjanovic D 2009 *J. Appl. Phys.* **105** 094102
[25] Dausch D E, Furman E, Wang F and Haertling G H 1996 *Ferroelectrics* **177** 221
[26] Dausch D E, Furman E, Wang F and Haertling G H 1996 *Ferroelectrics* **177** 237
[27] Lee D S, Lim D H, Kim M S, Kim K H and Jeong S J 2011 *Appl. Phys. Lett.* **99** 062906
[28] Su Lee D, Jong Jeong S, Soo Kim M and Hyuk Koh J 2012 *J. Appl. Phys.* **112** 124109
[29] Newnham R E, Skinner D P and Cross L E 1978 *Mater. Res. Bull.* **13** 525
[30] Groh C, Jo W and Rödel J 2014 *J. Am. Ceram. Soc.* **97** 1465
[31] Groh C, Franzbach D J, Jo W, Webber K G, Kling J, Schmitt L A, Kleebe H J, Jeong S J, Lee J S and Rödel J 2014 *Adv. Funct. Mater.* **24** 356
[32] Ayrikyan A, Weyland F, Steiner S, Duerrschnabel M, Molina-Luna L, Koruza J and Webber K G 2017 *J. Am. Ceram. Soc.* **100** 3673
[33] Ayrikyan A, Prach O, Khansur N H, Keller S, Yasui S, Itoh M, Sakata O, Durst K and Webber K G 2018 *Acta Mater.* **148** 432
[34] Ayrikyan A, Rojas V, Molina-luna L, Acosta M, Koruza J and Webber K G 2015 *IEEE Trans. Ultrason. Ferroelectr. Freq. Control* **62** 997
[35] Zhang H, Groh C, Zhang Q, Jo W, Webber K G and Rödel J 2015 *Adv. Electron. Mater.* **1** 1500018
[36] Chen D and Kamlah M 2015 *Rev. Sci. Instrum.* **86** 113707
[37] Segouin V, Domenjoud M, Bernard Y and Daniel L 2019 *J. Eur. Ceram. Soc.* **39** 2091
[38] Jo W and Rödel J 2011 *Appl. Phys. Lett.* **99** 2012
[39] Lynch C S 1996 *Acta Mater.* **44** 4137
[40] Tan X, Frederick J, Ma C, Aulbach E, Marsilius M, Hong W, Granzow T, Jo W and Rödel J 2010 *Phys. Rev.* B **81** 014103
[41] Takasaka S, Tsujimi Y and Yagi T 2002 *Phys. Rev.* B **65** 174102
[42] Dittmer R, Jo W, Rödel J, Kalinin S and Balke N 2012 *Adv. Funct. Mater.* **22** 4208
[43] Zhang S-T, Kounga A B, Aulbach E, Granzow T, Jo W, Kleebe H-J and Rödel J 2008 *J. Appl. Phys.* **103** 034107
[44] Xu C, Lin D and Kwok K W 2008 *Solid State Sci.* **10** 934
[45] Martin A, Khansur N H, Riess K and Webber K G 2019 *J. Eur. Ceram. Soc.* **39** 1031
[46] Franzbach D J 2014 Field induced phase transitions in ferroelectric materials *PhD Thesis* Technical University of Darmstadt
[47] Kounga Njiwa A B, Aulbach E, Granzow T and Rödel J 2007 *Acta Mater.* **55** 675
[48] Granzow T, Leist T, Kounga A B, Aulbach E and Rödel J 2007 *Appl. Phys. Lett.* **91** 142904
[49] Cai W, Wang P and Fan J 2020 *Mech. Mater.* **145** 103391
[50] Li X, Chen G, Chen X, Lu G-Q, Wang L and Mei Y-H 2012 *Solder. Surf. Mt. Technol.* **24** 120
[51] Paul S, Motalab M, Zubaer M A and Hossain M Z 2017 *J. Adhes. Sci. Technol.* **31** 1782
[52] Vögler M, Novak N, Schader F H and Rödel J 2017 *Phys. Rev.* B **95** 024104
[53] Dittmer R, Jo W, Webber K G, Jones J L and Rödel J 2014 *J. Appl. Phys.* **115** 084108